Coefficient of Performance Optimization of Single-Effect Lithium-Bromide Absorption Cycle Heat Pumps

Vinther, Kasper; Just Nielsen, Rene; Nielsen, Kirsten Mølgaard; Andersen, Palle; Pedersen, Tom Søndergård; Bendtsen, Jan Dimon

Published in:
IEEE Conference on Control Applications (CCA), 2015

DOI (link to publication from Publisher):
10.1109/CCA.2015.7320838

Publication date:
2015

Document Version
Early version, also known as pre-print

Coefficient of Performance Optimization of Single-Effect Lithium-Bromide Absorption Cycle Heat Pumps

Kasper Vinther[1], Rene J. Nielsen[2], Kirsten M. Nielsen[1], Palle Andersen[1], Tom S. Pedersen[1] and Jan D. Bendtsen[1]

Abstract— **In this paper, we investigate the coefficient of performance (COP) of a LiBr absorption cycle heat pump under different operating conditions. The investigation is carried out using a dynamical model fitted against data recorded from an actual heat pump used for district heating in Sønderborg, Denmark. Since the model is too complex to study analytically, we vary different input variables within the permissible operating range of the heat pump and evaluate COP at the resulting steady-state operating points. It is found that the best set-point for each individual input is located at an extreme value of the investigated permissible range, and that the COP optimization is likely to be a convex problem. Further, we exploit this observation to propose a simple offline set-point optimization algorithm, which can be used as an automated assistance for the plant operator to optimize steady-state operation of the heat pump, while avoiding crystallization issues.**

I. Introduction

In Denmark there has been an increasing interest for using geothermal energy as a supplemental resource for central heating and power plants. Unlike e.g., Iceland (see [1]), the temperature of geothermal water in Denmark is too low for direct use in district heating (DH); hence the temperature must be raised, e.g. using a heat pump. Due to Danish taxation laws it is particularly economically beneficial to use an absorption cycle heat pump (ACHP) in which relatively low valued heat can substitute the high valued electrical energy necessary in other heat pumps

ACHPs contain a binary solution consisting of a refrigerant and an absorbent. A commonly used combination of refrigerant and absorbent is water and Lithium-Bromide (LiBr). The working principle is as follows. Water is evaporated in an evaporator using heat from a low temperature heat source, e.g., geothermal energy. The water steam is then absorbed in a water-LiBr solution in an absorber, which expels heat to the surroundings, e.g., DH water, in an exothermic process. The solution is then pumped to a generator, where a desorption process occurs using a high temperature heat source. The concentrated solution is then fed back to the absorber and the generated water steam is condensed in a condenser, which expels heat to the surroundings, e.g., DH water. the condensed water is then finally returned to the evaporator. A more thorough description is found in, e.g., [2], [3].

For economic and environmental reasons it is desirable to operate the ACHP as efficient as possible. A way to quantify the efficiency is to calculate the ratio between useful heat output and required heat/power input, also known as the coefficient of performance (COP). An extensive investigation of COP is carried out in [4] for different sorbent/refrigerant working pairs, single-effect to triple-effect systems, and different applications including heat pumping. COP and thermodynamic characteristics of different working pairs are also investigated in [5] for air-conditioning applications on a simple steady state model. Additionally, [6] provide a few steady-state COP maps as a function of different operating conditions for an absorption refrigeration system. The references [4], [5], [6] indicate that good results in terms of COP can be obtained for the working pair water-LiBr. However, dynamics are not considered and the contributions are mostly directed towards the system design phase.

The ACHP setup considered in [7] is closer to a DH setup, where waste heat is used in the evaporator. The authors have investigated the effect of changes in different inputs on COP. They also emphasize that including dynamics in the modeling of ACHP is important to be able to describe part-load operation, because changes in one input can give rather complex changes in other parts of the system. Further, using a water-LiBr solution introduces the risk of crystallization if the LiBr concentration gets too high, which can block the solution flow in the system very quickly and thus halt operation. However, the results in [7] do not include investigation of where the boundary of operation is or proposal of any method to find the optimal operating conditions. Different strategies to avoid crystallization are discussed in [8], [9], [10], but they do not consider optimization of operating conditions. An ACHP is modeled using neural networks and optimized using genetic algorithms in [11]. Good results are obtained, but these methods tend to be rather complex, non-transparent, and no clear indication of the effect of each input on COP is provided. They potentially also use conservative constraints on inputs to prevent crystallization.

In this paper it is analyzed how the COP depends on the working conditions for a specific heat pump in a DH setup with geothermic energy as heat source, situated at Sønderborg in Southern Denmark. The aim is to be able to use this knowledge in general to suggest set-points for existing heat pump control loops in order to optimize the operation. Note, however, that the tuning of such existing

*This work was financially supported by the Danish Energy Agency through the EUDP project GreenFlex (jn:64013-0133) and the Faculty of Engineering and Science at Aalborg University

[1]K. Vinther, K. Nielsen, P. Andersen, T. Pedersen and J. Bendtsen are with the Section of Automation and Control, Department of Electronic Systems, Aalborg University, 9220 Aalborg, Denmark {kv,kmn,pa,tom,dimon}@es.aau.dk

[2]R. Nielsen is with Added Values, 7100 Vejle, Denmark RJN@AddedValues.eu

feedback control loops is beyond the scope of the present paper. The results are based on a nonlinear dynamic simulation model described in [12], where the model parameters are adjusted to measurements from the actual heat pump and give a fair accuracy in the operating area. A dynamic model is used to also capture the effect of changes in set-points on potential LiBr crystallization issues. Both a general unconstrained case, where all potential inputs to the heat pump are varied independently, and a specific constrained DH case is considered. The investigation of COP is based on changes in the working conditions implemented as feasible changes in the references to the low-level control loops already in place at the plant. A specific optimization is proposed, which uses a simple bisection algorithm to search for set-points that do not violate a crystallization boundary. Further, suggestions for smooth transitions between set-points are provided.

The rest of the paper is organized as follows. In Section II, the DH ACHP set-up is described. Section III presents a brief overview of the model of the ACHP used for the optimization. Section IV gives an analysis of the ACHP COP. Section V presents a method for optimizing the operating conditions to achieve better COP, and finally section VI draws some conclusions.

II. District Heating Heat Pump Setup

As stated, the setup considered in this paper is modeled based on a actual Danish DH supply system. That system contains, among others, four interconnected ACHPs; however, the following analysis is limited to only include a model of the largest of these heat pumps. All heat pumps are delivered by Hope Deepblue Air-conditioner Manufacture Corp., Ltd., and the heat pump in question has an operational weight of 67 ton [13] with a heat transfer rate in the evaporator of up to 6.5 MW. Figure 1 shows an illustration of the considered ACHP setup.

Some of the DH water from the city first enters the absorber and the small cooling heat exhanger (HEX), which both heat up the water. Some of the DH water then enters the condenser, giving an additional temperature increase. Finally, an additional heating occurs in the hot HEX, if the water has not reached the target forward temperature $T_{23,r}$ of ∼75–82°C (the exact value depends on the season). The temperature of the water that enters the absorber T_{13} will, in the specific case here, be approximately 10–15°C higher than the return water from the city (∼42°C), because it has passed the three other smaller heat pumps beforehand.

The low temperature heat source used in the evaporator is in fact DH water from the city, which is later reheated by hot water from a geothermal well at ∼48°C. This is therefore considered as a "free" source of energy, since COP is calculated from the net added energy to the DH water. The high-temperature water used in the generator and the hot HEX is generated by wood-chip fired boilers and is ∼170°C. The objective in terms of energy optimization is therefore to heat up the DH water using a minimal amount of high-temperature water.

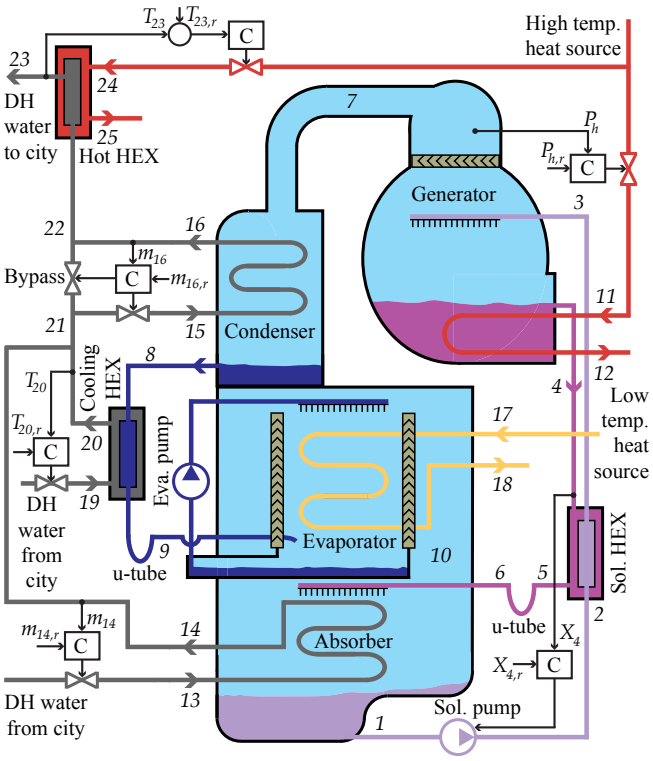

Fig. 1. Illustration of an absorption cycle heat pump in a district heating setup. Controllers are indicated with a C and the numbers indicate thermodynamic state points (used in the subscript notation on variables).

The flow of geothermal water and the city heat demand determines the baseline evaporator mass flow m_{18} (capacity utilization of the heat pump). The heat pump is then specified to operate with external absorber (m_{14}) and condenser (m_{16}) mass flows within a certain scaling range of the evaporator mass flow with the following min and max margins;

$$0.95k_a m_{18} \leq m_{14} \leq 1.6k_a m_{18}, \quad (1)$$

$$0.85k_c m_{18} \leq m_{16} \leq 1.15k_c m_{18}, \quad (2)$$

with absorber flow scaling constants $k_a = 1.591$ and condenser flow scaling $k_c = 1.078$. These scalings are determined by the manufacturer of the heat pump and used as a guideline to ensure stable operation of the absorption cycle, where the LiBr/water solution does not crystallize due to a too high concentration. The mass flow through the additional cooling HEX m_{20} is controlled to maintain a fixed outlet temperature T_{20}.

In addition to the external mass flow controls, there are also some internal heat pump feedback control loops. The solution pump ensures a suitable generator LiBr concentration X_4 by circulating more weak solution from the absorber if the concentration in the generator gets too high. The generator and condenser operate at a higher pressure than the evaporator and absorber. The high pressure P_h is maintained by regulating the mass flow of hot water through the generator, which produces steam. These two feedback loops are implemented using PI controllers and are considered to be supplied by the heat pump manufacturer.

A mechanical design with overflow and u-tube mechanisms in the generator and condenser help to keep suitable liquid levels in the generator and condenser and thus a suitable mass distribution in the system. The u-tubes also help to maintain a pressure difference between the low and high pressure side. For further explanation of the u-tube design see [9] and further analysis of the internal heat pump control structure can be found in [14]. Finally, the evaporator pump is used to circulate water over the evaporator HEX in order to maintain a constant production of steam. However, operation of this pump is not considered in the following. Further, only normal heat pump operation is considered and start/stop procedures are therefore neglected.

III. Absorption Cycle Heat Pump Model

The dynamic ACHP model used in this work is based on mass and energy balances and thermodynamic property functions. Further, the model is implemented in the *Modelica* modeling language. A detailed derivation of the model was given in [12] and a summary is provided in the following.

The four main components are evaporator, absorber, generator, and condenser. In the following it is assumed that the evaporator and absorber operate at the same low pressure, and that the generator and condenser operate at the same high pressure. Further, there are no heat losses to the ambient air and each of the four main components can be represented by a liquid control volume (subscript l) and a vapour control volume (subscript v). The overall mass balances are

$$\text{Eva:} \quad \frac{dM_e}{dt} = m_9 - m_{10}, \tag{3}$$

$$\text{Abs:} \quad \frac{dM_a}{dt} = m_6 + m_{10} - m_1, \tag{4}$$

$$\text{Gen:} \quad \frac{dM_g}{dt} = m_3 - m_4 - m_7, \tag{5}$$

$$\text{Con:} \quad \frac{dM_c}{dt} = m_7 - m_8, \tag{6}$$

$$M_i = V_{i,l}\rho_{i,l} + V_{i,v}\rho_{i,v} = V_{i,l}\rho_{i,l} + (V_{i,tot} - V_{i,l})\rho_{i,v} \tag{7}$$

where M is mass, V is volume, ρ is density, m is mass flow, $i \in \{e, a, g, c\}$ in (7) and (14) denote each component, and subscript tot denotes total. The LiBr mass balances are

$$\text{Abs:} \quad \frac{d\left(X_a V_{a,l}\rho_{a,l}\right)}{dt} = X_6 m_6 - X_1 m_1, \tag{8}$$

$$\text{Gen:} \quad \frac{d\left(X_g V_{g,l}\rho_{g,l}\right)}{dt} = X_3 m_3 - X_4 m_4, \tag{9}$$

where X is mass fraction of LiBr. The energy balances are

$$\text{Eva:} \quad \frac{dU_e}{dt} = m_9 h_9 - m_{10} h_{10} + Q_e, \tag{10}$$

$$\text{Abs:} \quad \frac{dU_a}{dt} = m_6 h_6 + m_{10} h_{10} - m_1 h_1 - Q_a, \tag{11}$$

$$\text{Gen:} \quad \frac{dU_g}{dt} = m_3 h_3 - m_4 h_4 - m_7 h_7 + Q_g, \tag{12}$$

$$\text{Con:} \quad \frac{dU_c}{dt} = m_7 h_7 - m_8 h_8 - Q_c, \tag{13}$$

$$U_i = V_{i,l}\rho_{i,l}h_{i,l} + V_{i,v}\rho_{i,v}h_{i,v} - p_i V_{i,tot} \tag{14}$$

where U is internal energy, Q is heat transfer rate, h is specific enthalpy, and p is pressure. Additionally, the mass and energy balances are supplemented with thermodynamic property functions for steam/water and LiBr solutions.

The water vapor flow out of the generator solution and the water vapor flow absorbed in the absorber are driven by the amount of heat transferred through the HEXs assuming that the solutions are always in a saturated state. It is also assumed (see [2]) that the solution that exits the absorber and generator, the water that exits the condenser, and the vapor that exits the evaporator, all are in a saturated state (same state as in the respective components). Additionally, the vapor from the generator interacts with the solution from the absorber in a counterflow way (sprayed in), such that the vapor at the outlet is superheated to the saturation temperature of the solution, see again [2].

The heat exchange in the four main components as well as in the water HEX and the solution HEX, shown in Fig. 1, are too complicated to model with simple lumped-parameter models. Instead, the heat transfer is modeled using 1-dimensional dynamic staggered grid flow models in a finite volume representation with N volume elements (uniformly distributed) and $N+1$ flow elements in between the volumes. Details of the staggered grid models can be found in [12], along with descriptions of the valve and pump models.

IV. Heat Pump COP Analysis - Unconstrained Case

If the low temperature heat source used in the evaporator is considered as a "free" source of energy and if we only consider the net energy delivered to the DH water by the ACHP versus the required energy in the generator, then an unconstrained coefficient of performance COP_u can be defined as

$$COP_u = \frac{Q_a + Q_c + Q_{ch}}{Q_g}, \tag{15}$$

where Q_g, Q_a, Q_c, and Q_{ch} are the heat transfer rates between the external water flows and the generator, absorber, condenser, and cooling HEX, calculated as;

$$Q_g = m_{12}\left(h_{11} - h_{12}\right), \tag{16}$$

$$Q_a = m_{14}\left(h_{14} - h_{13}\right), \tag{17}$$

$$Q_c = m_{16}\left(h_{16} - h_{15}\right), \tag{18}$$

$$Q_{ch} = m_{20}\left(h_{20} - h_{19}\right), \tag{19}$$

where the subscript numbers in mass flows m and specific enthalpy h refer to Fig. 1. The specific enthalpies are calculated using property function tables for water, with pressure and temperature as inputs. Note that (16)-(19) can be calculated solely using measurements of the external water flows (no internal ACHP measurements) and that COP_u is unconstrained in the sense that external connections of the DH water flow are not considered, e.g., that the outlets of the absorber and cooling HEX are not connected to the inlet of the condenser. Further, the electrical consumption of the pumps is very small compared to the heat transfers and

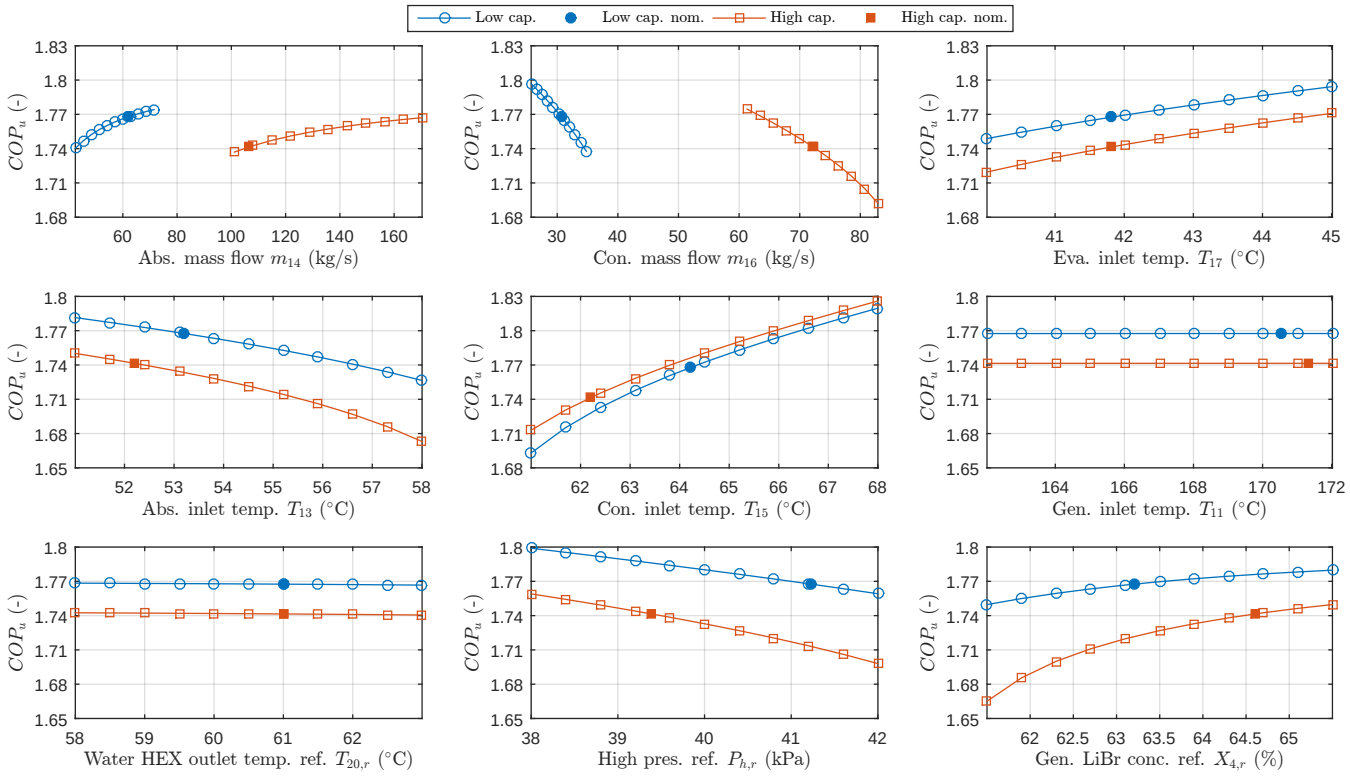

Fig. 2. Plot of different variables effect on the unconstrained COP, defined in (15), while keeping the other variables at their nominal values. Low and high capacity nominal situations are defined by data from a heat pump at Sønderborg DH.

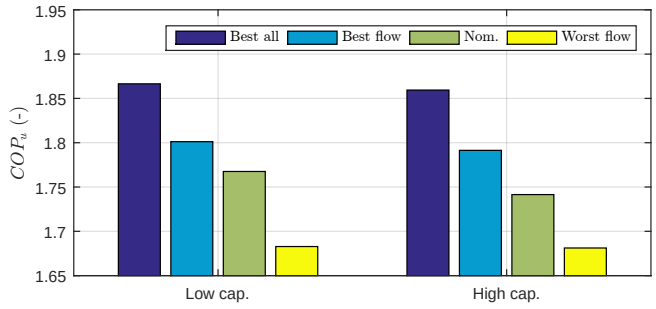

Fig. 3. Unconstrained COP when the set-point with highest COP for each variable is chosen (best all), when the combination of absorber and condenser flow with highest COP is chosen (best flow), when the opposite flow is chosen (worst flow), and compared with the nominal situation (nom.).

TABLE I

PERCENTAGE IMPROVEMENT IN COP BETWEEN WORST AND BEST SET-POINT FOR DIFFERENT VARIABLES OF INTEREST. RESULTS AT BOTH LOW AND HIGH CAPACITY ARE SHOWN.

Paramter	ΔCOP_u (%) Low capacity	ΔCOP_u (%) High capacity
Abs. mass flow m_{14}	1.94	1.73
Con. mass flow m_{16}	3.40	4.87
Gen. inlet temp. T_{11}	0.00215	0.00216
Abs. inlet temp. T_{13}	3.18	4.61
Con. inlet temp. T_{15}	7.48	6.60
Eva. inlet temp. T_{17}	2.60	2.99
Water HEX temp. ref. $T_{20,r}$	0.0975	0.112
High pres. ref. $P_{h,r}$	2.26	3.59
Gen. LiBr conc. ref. $X_{4,r}$	1.72	5.08
Best all vs nom.	5.60	6.77
Best all vs worst flow	10.91	10.60

can be assumed to be negligible. This analysis is performed to investigate how each of the inputs affect the performance of the ACHP.

Fig. 2 shows steady state COP_u as a function of changes in different inputs. Eleven values of each input is simulated on the ACHP model, while the other inputs are held constant in their nominal values. Both a low and a high capacity situation are shown for comparison. The operating conditions at these capacities are defined by data from the actual heat pump. The evaporator mass flow was 28.1 kg/s during low capacity and 66.9 kg/s during high capacity (notice that the absorber and condenser flows are scaled according to the evaporator flow, which explains the different investigated ranges). The results are further elaborated in Fig. 3, where the nominal COP_u is compared with a situation where all inputs are chosen according to their best values (best all) and when just the absorber and condenser flow are chosen as their best values (best flow) and worst values (worst flow). Additionally, Table I shows the percentage improvement in COP_u between the worst and best set-point for the inputs. The absorber and condenser flow ranges are given by (1)-

(2) and the range for temperatures and references are chosen within realistic values based on data from the actual ACHP.

The results show that the best set-point for each individual input is located at an extreme value for the investigated ranges and that all the curves are monotonic and concave, which are good properties for optimization. A relatively small change in COP_u is observed between the best and the worst set-points for the generator inlet and water HEX outlet temperatures. The rest of the input variables have a larger impact on COP_u for the tested operating ranges. Further, the "best all" scenario showed an improvement in COP_u of approximately 6% when compared with the "nominal" scenario and 11% when compared with the "worst flow" scenario. Note that the "best all" scenario only uses the individual best set-points, which do not necessarily correspond to the best overall operating conditions.

The absorber and condenser flow ranges recommended by the manufacturer are conservatively chosen, in order to account for different inlet temperatures. Further optimization could be obtained if larger flexibility in ranges are allowed. For healthy operation of the heat pump it is important that crystallization is avoided. A piecewise polynomial function is fitted to manufacturer data and defines the LiBr/water solution temperature $T_{c,l}$, at which the solution starts to crystallize, as a function of LiBr concentration X:

$$T_{c,l} = \begin{cases} 0.0533X^3 - 10.2X^2 \\ \quad +653X - 13978 & \text{if } X < 64.7 \\ -0.636X^2 + 97.8X - 3.62 & \text{otherwise} \end{cases} \tag{20}$$

If the temperature drops below the limit then crystals will start to form. Equation (20) can therefore be used to check the validity of set-points and Fig. 4 shows a plot of (20) together with a 5°C margin to account for uncertainties and disturbances. The critical point in terms of crystallization is located where the strong solution from the generator enters the absorber [8], because the solution temperature is lowest here. The critical point is also plotted in Fig. 4 for the simulations presented in Fig. 3 (best all, best flow, nom., worst flow). The "best all" scenario operates closest to the crystallization bound, which indicates that the optimal operating condition is located on the 5°C margin curve.

V. District heating heat pump COP Optimization

Each of the inputs considered in Section IV are not independent in the DH setup. If the case presented in Fig. 1 is instead considered, then the outlets of the absorber and the cooling HEX are connected to the inlet of the condenser and a hot HEX is used to reach a certain target DH water temperature. In this constrained case we can define a coefficient of performance as

$$COP_c = \frac{Q_a + Q_c + Q_{ch} + Q_{hh}}{Q_g + Q_{hh}}, \tag{21}$$

where Q_g, Q_a, Q_c, and Q_{ch} are defined as in (16)-(19) and Q_{hh} is the required heat transfer rate in the hot HEX in order

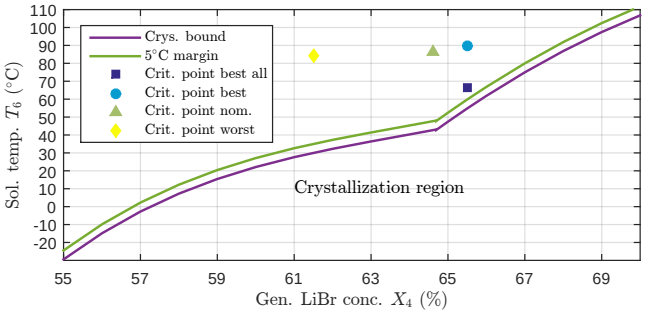

Fig. 4. Plot of the LiBr crystallization boundary and a 5°C margin as a function of generator LiBr concentration X_4 and solution temperature T_6 (most critical thermodynamic state point in the cycle). The marked points are from the simulation results shown in Fig. 3.

to reach a certain outlet DH water temperature;

$$Q_{hh} = m_{23}\left(h_{23} - h_{22}\right). \tag{22}$$

Then the goal in an optimization problem can be formulated as to maximize COP_c or minimize the usage of $Q_g + Q_{hh}$, while still obtaining the target DH water outlet temperature T_{23} and avoiding crystallization of LiBr.

The above optimization goal is investigated in the following, where two optimization variables are considered; the condenser mass flow m_{16} and the generator LiBr concentration X_4. The condenser mass flow is chosen because it is possible to control the amount of water, which bypasses the condenser, and because it is assumed that the mass flow and inlet temperature at the absorber and evaporator is determined elsewhere in the system (determined by the flow in the geothermal well and the operation of the other heat pumps). Furthermore, choosing the LiBr concentration makes it possible to operate close the crystallization boundary, which the analysis in Section IV indicated as a good operating point in terms of maximizing COP. Two variables also provides a relatively simple optimization problem, which can be visualized with 3D plots. However, higher dimension problems could be considered as well.

Fig. 5 shows the steady state constrained COP as a function of condenser mass flow and generator LiBr concentration in the high capacity situation (a), in the high capacity situation with higher absorber inlet temperature (b), and in the low capacity situation (c). Simulations that violated the 5°C crystallization margin are marked with red stars. In all cases the optimum is located at the highest allowed condenser flow and at the LiBr concentration closest to the crystallization margin.

This information can be used in a simple search algorithm with the pseudo-code provided in Algorithm 1. Note that a bisection search is used to lower the required number of simulation runs of the nonlinear dynamic heat pump model (one iteration in the algorithm takes approximately 5-10 seconds on a standard laptop). The proposed optimization could also have been performed with other convex solution methods such as the simplex algorithm or the Newton-Raphson method. Note further that offline optimization is

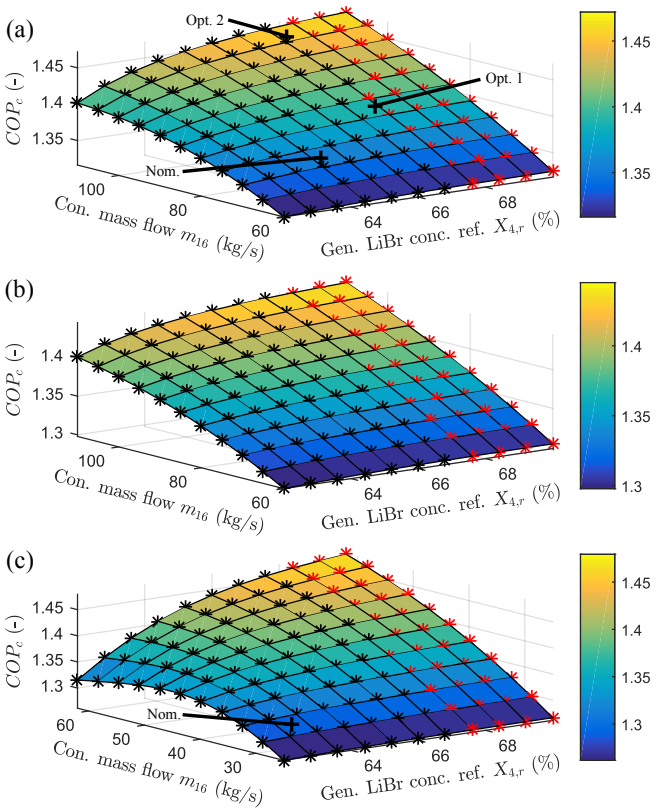

Fig. 5. Constrained COP for different combinations of condenser mass flow and generator LiBr concentration under the nominal high capacity situation with indication of optimal points 1 and 2 (a), under the high capacity situation with a 5°C higher absorber inlet temperature T_{13} (b), and under the nominal low capacity situation (c). The red data points indicate simulations where the crystallization margin is violated.

TABLE II

COP, PERCENTAGE IMPROVEMENT IN COP BETWEEN NOMINAL AND OPTIMIZED SET-POINTS, AND HIGH TEMPERATURE HEAT USAGE.

Parameter	COP_c	ΔCOP_c vs. nom. (%)	$Q_g + Q_{hh}$ (MW)
Nom.	1.361	0	10.07
Opt. 1	1.398	2.74	9.82
Opt. 2	1.458	7.11	9.46

Initialize model with measured operational data;
Set maximum search range for optimization vars
$m_{16} = \{m_{16,min}, m_{16,max}\}$
$X_{4,r} = \{X_{4,r,min}, X_{4,r,max}\}$;
while *i < max iterations* **do**
  Simulate model to steady state;
  Compute crystrallization limit temp. $T_{c,l}$;
  if *Sol. temp.* $T_6 >$ *lower limit* $T_{c,l}$ **then**
    Save current m_{16} as potential set-point;
    $m_{16,min} = m_{16}$;
  else
    $m_{16,max} = m_{16}$;
  end
  $m_{16} = (m_{16,max} - m_{16,min})/2$;
  i++;
end
Repeat procedure for $X_{4,r}$ with saved m_{16} set-point;

Algorithm 1: Set-point search

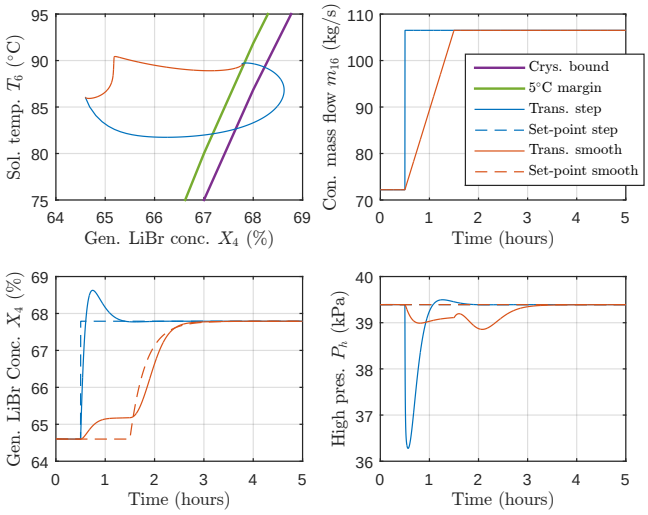

Fig. 6. Simulation results using either a step or a smooth change in set-points going from the nominal situation to the optimal point 2.

often acceptable in practice due to the fact that the ACHP operates under steady-state conditions for extended periods of time. Should the ACHP be subject to changing load conditions, one may of course consider online approaches such as model predictive control instead.

The search finds optimum point 1 (Opt. 1) if the maximum condenser flow is limited according to (2) and finds optimum point 2 (Opt. 2) if the maximum condenser flow is equal to the absorber flow, see Fig. 5 (a). These results are further elaborated in Table II.

A 2.74% increase in COP in Opt. 1 and a 7.11 % increase in COP in Opt. 2 is observed relative to nominal operation. The increase in COP also means a reduction in the high temperature source heat transfer rate ($Q_g + Q_{hh}$) of 0.25 MW in the simulated case. This has a large potential impact on operational costs as this heat source is driven by wooden-chips or gas if a gas-fired boiler is used. The high condenser flow case (Opt. 2) showed an even higher reduction of 0.61 MW, while also avoiding crystallization and still meeting the forward temperature demand with the same DH water flow.

Application of the new optimized set-points in closed loop, both as a step change and as smooth transitions, are shown in Fig. 6. It is assumed that mass flows can be changed momentarily (fast dynamics) and that pressure and concentration are controlled with PI loops (see control loops in Fig. 1). The step changes gives an overshoot in X_4, which results in violation of the crystallization bound. If the condenser mass flow is instead ramped up first, followed by a first order filtering of $X_{4,r}$, then a smoother transition is obtained without overshoot (notice how the simulation converges to a point (T_6, X_4) on the crystallization margin). A smaller disturbance is also observed in the high pressure

using the smooth transition. This shows the importance of checking the transition using a dynamic model.

VI. Conclusion

In this paper, we investigated the COP of a single-effect LiBr ACHP under different operating conditions. The investigation was carried out using a dynamical model developed earlier for control purposes and fitted against data recorded from an actual heat pump used for DH in Sønderborg, Southern Denmark.

In the study, we systematically varied different variables within the permissible operating range. The results show that the best set-point for each individual input is located at an extreme value for the investigated ranges and that all the COP curves illustrated on Fig. 2 are monotonic and concave. Thus, it is highly likely that the COP optimization problem remains convex even if several inputs are included as decision variables, and convex methods for multi-dimensional optimization could be effective. We illustrated this by evaluating COP for intervals of condenser mass flow and generator LiBr concentration.

The results presented in this paper involve steady-state operating conditions, which is reasonable since ACHPs are typically not intended for rapid load changes and similar transient behavior. However, as illustrated by a simulation in Section V, the dynamics involved in controlling the ACHP to the optimal operating conditions cannot be ignored entirely.

Future work involves integrating all four ACHPs in Sønderborg and optimizing their combined operation, along with dynamic control in accordance with the static set-point analysis discussed in the present paper.

References

[1] G. Axelsson, E. Gunnlaugsson, T. Jonasson, and M. Olafsson, "Low-temperature geothermal utilization in iceland - decades of experience," *Geothermics*, vol. 39, pp. 329–338, 2010.

[2] K. E. Herold, R. Radermacher, and S. A. Klein, *Absorption Chillers and Heat Pumps*. CRC Press, 1996.

[3] P. Srikhirin, S. Aphornratana, and S. Chungpaibulpatana, "A review of absorption refrigeration technologies," *Renewable Sustainable Energy Rev.*, vol. 5, no. 4, pp. 343–372, 2001.

[4] M. Pons, F. Meunier, G. Cacciola, R. E. Critoph, M. Groll, L. Puigjaner, B. Spinner, and F. Ziegler, "Thermodynamic based comparison of sorption systems for cooling and heat pumping," *Int. J. Refrig.*, vol. 22, no. 1, pp. 5–17, 1999.

[5] V. H. F. Flores, J. C. Román, and G. M. Alpíres, "Performance Analysis of Different Working Fluids for an Absorption Refrigeration Cycle," *American J. of Env. Eng.*, vol. 4, no. 4A, pp. 1–10, 2014.

[6] D.-W. Sun, "Thermodynamic Design Data and Optimum Design Maps for Absorption Refrigeration Systems," *Appl. Therm. Eng.*, vol. 17, no. 3, pp. 211–221, 1997.

[7] S. Jeong, B. Kang, and S. Karng, "Dynamic Simulation of an Absorption Heat Pump for Recovering Low Grade Waste Heat," *Appl. Therm. Eng.*, vol. 18, no. 1-2, pp. 1–12, 1998.

[8] X. Liao and R. Radermacher, "Absorption chiller crystallization control strategies for integrated cooling heating and power systems," *Int. J. Refrig.*, vol. 30, no. 5, pp. 904–911, 2007.

[9] Y. Shin, J. A. Seo, H. W. Cho, S. C. Nam, and J. H. Jeong, "Simulation of dynamics and control of a double-effect LiBr-H2O absorption chiller," *Appl. Therm. Eng.*, vol. 29, no. 13, pp. 2718–2725, 2009.

[10] K. Wang, O. Abdelaziz, P. Kisari, and E. A. Vineyard, "State-of-the-art review on crystallization control technologies for water/LiBr absorption heat pumps," *Int. J. Refrig.*, vol. 34, no. 6, pp. 1325–1337, 2011.

[11] T. T. Chow, G. Q. Zhang, Z. Lin, and C. L. Song, "Global optimization of absorption chiller system by genetic algorithms and neural network," *Energy Build.*, vol. 34, no. 1, pp. 103–109, 2002.

[12] K. Vinther, R. J. Nielsen, K. M. Nielsen, P. Andersen, T. S. Pedersen, and J. D. Bendtsen, "Absorption Cycle Heat Pump Model for Control Design," in *ECC*, Linz, Austria, July 2015, in press.

[13] Hope Deepblue Air Conditioning Manufacture Corp., Ltd. (2014, Sep.) Hot water-type libr absorption chiller. [Online]. Available: http://www.slhvac.com/productsinfo.aspx?NId=8&NodeID=15

[14] K. Vinther, R. J. Nielsen, K. M. Nielsen, P. Andersen, T. S. Pedersen, and J. D. Bendtsen, "Analysis of Decentralized Control for Absorption Cycle Heat Pumps," in *ECC*, Linz, Austria, July 2015, in press.